Use of ground-based signals of opportunity for smart projectile navigation

J Wright and **M Costello***
School of Aerospace Engineering, Georgia Institute of Technology, Atlanta, Georgia, USA

The manuscript was received on 1 December 2009 and was accepted after revision for publication on 26 May 2010.

DOI: 10.1243/09544100JAERO751

Abstract: Global positioning system (GPS) is a widely accepted means of navigation, whether it is for civilian or military means. With the implementation of GPS on smart projectiles, these weapons have been able to achieve remarkable accuracy. Even though the improvements in accuracy are impressive, GPS signals are susceptible to jamming and spoofing by a sufficiently motivated enemy. The work reported here examines the viability of constructing a navigation solution using ground-based signals of opportunity that provide range and range rate information. Using a generalized sensor model encompassing the key error terms, a variety of physical devices are included in the analysis. For a typical indirect fire trajectory, navigation solutions are computed as a function of the number and density of signal sources, terrain type, and sensor errors. Results indicate that navigation solutions can be computed with the same accuracy as current GPS systems with a moderate number of signal sources. Generally, more accurate solutions are obtained when the projectile is directly over the signal sources and there is a variation of signal source location in all three axes.

Keywords: global positioning system, signals of opportunity, navigation, projectile, inertial measurement unit

1 INTRODUCTION

Global positioning system (GPS) is more and more a ubiquitous part of society. For more than a decade, smart indirect fire projectiles and smart bombs have employed GPS position and velocity feedback to achieve remarkable accuracy. An early example is the Joint Direct Attack Munition (JDAM). By employing GPS, the JDAM achieved a circular error probable (CEP) of 10 m (∼33 ft), which was demonstrated during Operation Allied Force, the NATO bombing of Yugoslavia in 1999 [**1**]. Another example is the Excalibur, a 155 mm extended range-guided artillery shell. Unguided, it possesses a CEP of 200–300 m at moderate ranges, where the GPS-guided derivative achieves a CEP of 10 m, an astonishing increase in accuracy and precision [**2**]. While these improvements in accuracy are impressive, they are accompanied by a substantial increase in cost and sophistication of the weapon. Moreover, one of the more worrisome aspects of GPS-enabled munitions is the fact that GPS signals can be easily jammed or spoofed by a sufficiently motivated enemy. A current method to mitigate GPS signal loss is to integrate an inertial navigation system (INS) along with a Kalman filter to obtain a navigation solution. Also, when GPS signals are available, this system allows a navigation solution to be computed at higher rates than GPS alone can provide. For example, JDAM employs an INS to ensure that should GPS be lost, the munition can still hit its target. Solely relying on INS, the JDAM has a CEP of 30 m, which is not as accurate as guidance by GPS but still provides sufficient accuracy [**1**].

A substantial amount of research has been performed on countering GPS jamming. A traditional approach to anti-jamming is to employ a six-antenna element arranged in a hexagonal pattern around a central reference element, where all elements are connected to a central electronics box that controls the phase and gain of each element. By tuning each of the antennas independently, a null can be placed in the direction of an undesired signal source. However, this concept is relatively large, 35 cm, and only

**Corresponding author: School of Aerospace Engineering, Georgia Institute of Technology, Atlanta, Georgia 30332, USA.*
email: mark.costello@ae.gatech.edu

works with a few unwanted signal sources [**3**]. Two current anti-jamming methods are jammer signal power reduction or frequency adaptive processing. Jammer signal power reduction employs space–time adaptive processing, where each antenna array element is delayed using a set of tapped delay lines. Once again, the major issues with power reduction is the fact that there are a limited number of degrees of freedom for which this concept will work and the need for multiple antennas [**3**]. Frequency adaptive processing is an adaptive narrowband process and uses only a single antenna element, ideal for smart weapons. These systems attempt to minimize measured power based on the assumption that any measured power must be a jamming signal [**4**]. However, it is only effective against structured interference signals and not broadband interference. Additionally, smart weapons have begun to utilize an INS as a method for navigating when GPS is jammed or denied. INSs utilize a set of accelerometers and gyroscopes which can then be integrated appropriately to estimate the states of projectile, such as position and velocity. Highly accurate inertial measurement units (IMUs) are expensive. Lower-cost and less accurate IMUs do find their way into smart weapons, but typically only as a backup should GPS signals be lost or jammed. Lower-cost IMUs can be built in-house or purchased as a relatively cheap alternative to more expensive models [**5**].

Another option for obtaining a navigation solution when GPS is not available is to use radio frequency (RF) signals of opportunity (SOOP) produced from known sources. Similar to GPS navigation systems, this concept utilizes known positions of ground-based signal sources and develops a pseudorange and pseudorange rate from the projectile to the source. By utilizing at least four sources, position and velocity can be computed. Savarese *et al.* demonstrated this concept via multiple experiments, using amplitude modification (AM) signals. They provide examples and results of using SOOP to accurately map an entire network [**6**]. Similarly, robots are using active and passive RFID signals to generate position and velocity information [**7**, **8**]. SOOP have been used by Air Force Institute of Technology in multiple research endeavours to explore the versatility of AM transmission band SOOP along with additional position tracking equipment [**9**–**11**]. Another well-demonstrated system employing this concept is eLORAN, which was recently chosen as the backup global navigation solution, should GPS be lost for an extended period of time. Currently, eLORAN allows for ± 8 m accuracy when roughly 165 km or less away from the transmitting towers [**12**–**14**].

This article explores the potential of creating a navigation solution for a smart projectile using an array of known ground-based RF sources that permit pseudorange and pseudorange rate information to be processed by a projectile in real time. Appropriate error levels were assumed and used to simulate errors in pseudorange and pseudorange rate signals. However, specific hardware details were not considered as it is a separate field of study, but it is assumed that the equipment exists and can be implemented on a projectile. The main focus of the article is exploring the effect of practical system features on the quality of the resulting navigation solution. The article begins with a description of the system geometry considered along with the numerical algorithm employed for constructing the navigation solution, including documenting the error model for range and range rate information. The algorithm is subsequently used to predict a navigation solution of a smart indirect fire projectile, flying a typical trajectory. Parametric trade studies considering the number of active signal sources, location of signal sources, density of signal sources, terrain types, and sensor error levels are conducted and contrasted with current GPS-based navigation solutions.

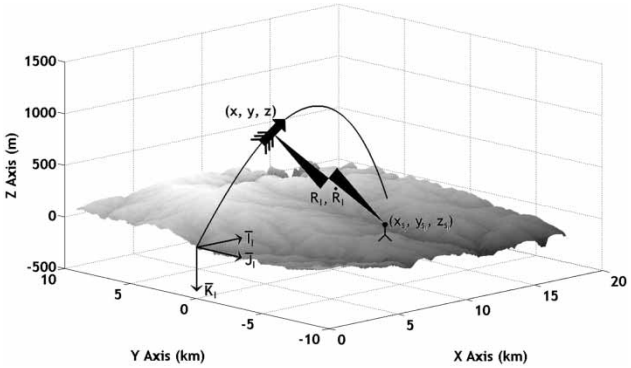

Fig. 1 System geometry for a single signal source

2 SYSTEM GEOMETRY

The scenario considered here consists of a projectile in atmospheric flight. The projectile is equipped with an electronics suite that processes measurements from n independent signal sources. For each signal source, the pseudorange and pseudorange rate from the projectile to the signal source is obtained at a given instant in time. The basic geometry is shown in Fig. 1. The inertial reference frame is fixed to the surface of the earth and is arranged so that its origin is located close to the gun muzzle with the $\bar{\boldsymbol{I}}_{\mathrm{I}}$ axis pointing down range. The $\bar{\boldsymbol{J}}_{\mathrm{I}}$ axis points to the right when viewed from the rear and the $\bar{\boldsymbol{K}}_{\mathrm{I}}$ axis points into the ground. The location of each signal source is known in the inertial reference frame.

The distance vector from the origin of the inertial frame to the mass centre of the projectile and the ith signal source is

$$\bar{\boldsymbol{r}}_{o\to p} = x\bar{\boldsymbol{I}}_{\mathrm{I}} + y\bar{\boldsymbol{J}}_{\mathrm{I}} + z\bar{\boldsymbol{K}}_{\mathrm{I}} \tag{1}$$

$$\bar{\boldsymbol{r}}_{o\to s_i} = x_{s_i}\bar{\boldsymbol{I}}_{\mathrm{I}} + y_{s_i}\bar{\boldsymbol{J}}_{\mathrm{I}} + z_{s_i}\bar{\boldsymbol{K}}_{\mathrm{I}} \tag{2}$$

while the corresponding translational velocities are

$$\bar{\boldsymbol{v}}_{\mathrm{P/I}} = \dot{x}\bar{\boldsymbol{I}}_{\mathrm{I}} + \dot{y}\bar{\boldsymbol{J}}_{\mathrm{I}} + \dot{z}\bar{\boldsymbol{K}}_{\mathrm{I}} \tag{3}$$

$$\bar{\boldsymbol{v}}_{S_i/\mathrm{I}} = \dot{x}_{s_i}\bar{\boldsymbol{I}}_{\mathrm{I}} + \dot{y}_{s_i}\bar{\boldsymbol{J}}_{\mathrm{I}} + \dot{z}_{s_i}\bar{\boldsymbol{K}}_{\mathrm{I}} \tag{4}$$

With these definitions, the range from the signal source to the associated projectile receiver is

$$|\bar{\boldsymbol{r}}_{o\to s_i} - \bar{\boldsymbol{r}}_{o\to p}| = R_i = \sqrt{(x-x_{s_i})^2 + (y-y_{s_i})^2 + (z-z_{s_i})^2} \tag{5}$$

and the range rate

$$\dot{R}_i = \frac{(x-x_{s_i})(\dot{x}-\dot{x}_{s_i}) + (y-y_{s_i})(\dot{y}-\dot{y}_{s_i}) + (z-z_{s_i})(\dot{z}-\dot{z}_{s_i})}{R_i} \tag{6}$$

3 NAVIGATION SOLUTION

The core signals used to create a navigation solution are the pseudorange and pseudorange rate from the signal source to the projectile receiver. Physically, this information can be extracted from an AM, television, cell phone tower, or radio beacon. The first method for determining the necessary information uses received signal strength indication, which employs the property that as a signal propagates in space the signal strength is reduced in a known manner, which in turn provides the distance between the signal source and receiver [**15**, **16**]. However, one drawback to this method is that the strength of the signals at their sources must be known beforehand. The second method utilizes time difference of arrival and multiple transmitters, synchronized in time. Using the synchronized transmitters, a navigation solution is determined by calculating the intersection of the hyperboles, which are generated due to the different distances between the transmitters and receiver [**17–19**]. Simulated pseudorange data are generated by adding noise and bias to the base signal as shown in equation (7). The symbol σ_i represents the standard deviation of the noise and w_i is random white noise. These are then multiplied together to produce a zero mean Gaussian noise with a standard deviation of σ_i

$$\tilde{R}_i = R_i(1 + \sigma_i w_i) + b_i \tag{7}$$

Equation (7) is a generalized sensor model that permits modelling many different physical sensors by properly setting the error characteristics (σ_i, b_i). Table 1 lists typical error values for several different signal sources.

The basic navigation solution problem is to determine $x, y, z, \dot{x}, \dot{y}, \dot{z}$ given a set of n measurements for R_i and $\dot{R}_i$. A vector of unknown parameters is defined as $P = [x\, y\, z]^{\mathrm{T}}$ and an error vector is defined by equation (8)

Table 1 Error characteristics for range and range rate [**7–9**, **12–14**, **20**]

	σ	b (m)
eLORAN (90–110 kHz)	0.000 08 – higher	0.3–3.0
AM (520–1710 kHz)	0.0001–0.0007	1.5–12.2
RFID (mHz)	0.001–0.01	0.2–0.5

$$\boldsymbol{E}_k = \begin{Bmatrix} (x_k - x_{s_1})^2 + (y_k - y_{s_1})^2 + (z_k - z_{s_1})^2 - \tilde{R}_1^2 \\ \vdots \\ (x_k - x_{s_n})^2 + (y_k - y_{s_n})^2 + (z_k - z_{s_n})^2 - \tilde{R}_n^2 \end{Bmatrix} \tag{8}$$

The non-linear algebraic error equations are solved by a standard Newton–Raphson method with a backtracking line search algorithm, where J_k is the Jacobian of the error residual

$$\boldsymbol{P}_{k+1} = \boldsymbol{P}_k - \alpha_k J_k^{-1}\boldsymbol{E}_k \tag{9}$$

$$J_k = \frac{\mathrm{d}\boldsymbol{E}_k}{\mathrm{d}\boldsymbol{P}_k} \tag{10}$$

The line search optimizer termination criteria are given as follows:

(a) $||\alpha_k J_k^{-1}\boldsymbol{E}_k||_2 \leqslant 0.0001$
(b) $||\boldsymbol{E}_k||_2 \leqslant (0.9||\boldsymbol{E}_1||_2)$
(c) $\alpha_k \leqslant (1/2)^{44}$

The first exiting criterion is due to the fact that the adjustment to the calculated position vector is so small that the additional increase in accuracy would not provide a much better navigation solution. The second criterion is based on the nature of the backtracking line search algorithm [**21**, **22**]. Finally, when alpha is below the third exiting criterion, the number would be so small that double precision codes could not accurately retain the integrity of the number.

To simulate an actual gun launch, the navigation algorithm is initiated after 1 s of flight time. This demonstrates the typical amount of time for the receiver to settle and produce navigation solutions. In order to start the navigation solver, an initial guess is required. The first ten individual guesses are provided via a simple closed-form solution based on launch conditions. After the first ten navigation solutions are calculated, a second-order polynomial is used, along with the ten previous navigation solutions, in order to compute an initial guess. This method is then utilized for the duration of the flight. If the Newton–Raphson method should not converge, trilateration is employed as a backup. Trilateration is a series of frame rotations and translations that can also be used to solve the non-linear navigation equations, in order to obtain position estimates [**23**, **24**]. Typically, the navigation solution rapidly converges. However, there are instances where

it does not converge, which usually occur directly after launch or right before impact.

Once the position solution is obtained from the range equations, the velocity solution can be obtained via linear least squares. Note, the signal sources were assumed to be stationary and $\dot{\tilde{R}}$ is an independent signal which is obtained via hardware on the projectile

$$\begin{bmatrix} \frac{x_k - x_{s_1}}{\tilde{R}_1} & \frac{y_k - y_{s_1}}{\tilde{R}_1} & \frac{z_k - z_{s_1}}{\tilde{R}_1} \\ \vdots & & \\ \frac{x_k - x_{s_n}}{\tilde{R}_n} & \frac{y_k - y_{s_n}}{\tilde{R}_n} & \frac{z_k - z_{s_n}}{\tilde{R}_n} \end{bmatrix} \begin{Bmatrix} \dot{x} \\ \dot{y} \\ \dot{z} \end{Bmatrix} = \begin{Bmatrix} \dot{\tilde{R}}_1 \\ \vdots \\ \dot{\tilde{R}}_n \end{Bmatrix} \quad (11)$$

In order to simulate decreased signal integrity via obstruction due to buildings, trees, and other structures, a line-of-sight algorithm is utilized to determine whether or not the projectile has a direct line of sight to the signal source. If there is no direct line of sight, the signal is not used in determining the navigation solution. This simulates logic on the projectile's receiver that if the signal strength drops below some threshold, then the signal is not used to calculate the current navigation solution.

4 EXAMPLE RESULTS

The M549 projectile used to examine the effectiveness of the navigation solution is a representative indirect fire, spin-stabilized projectile with a mass of 43 kg and length of 155 mm. Typical muzzle velocities are around 826 m/s with an associated spin rate of 1674 rad/s. At a quadrant elevation of 0.2239 rad, the M549 projectile travels roughly 14 km with a maximum altitude of 1120 m and an approximate cross range deviation of 88 m with 30 s of flight time. In order to generate these values and a nominal trajectory, a validated six-degrees-of-freedom model for a projectile, called BOOM, was used [**25**].

In order to document the typical performance for this type of navigation solution, an example simulation is presented below. The example uses 200 ground-based signals centred on the impact point of the nominal trajectory. In order to generate the signal locations, elevation data were acquired from the National Elevation Dataset (NED) to represent actual mission environments. An elevation data set for the Bonneville Salt Flats in Utah was used. It represents flat terrain as elevation varies 6 m over the entire 18.3 km × 18.3 km section of land. Figure 2 shows the location of the 200 signals plotted on the three-dimensional (3D) elevation data for this site. Sensor error characteristics used for this simulation are $\sigma = 0.0001$ and $b = 0.3$ m, which are representative of AM and or lower-frequency eLORAN signals. These values along with additional signal error levels can be

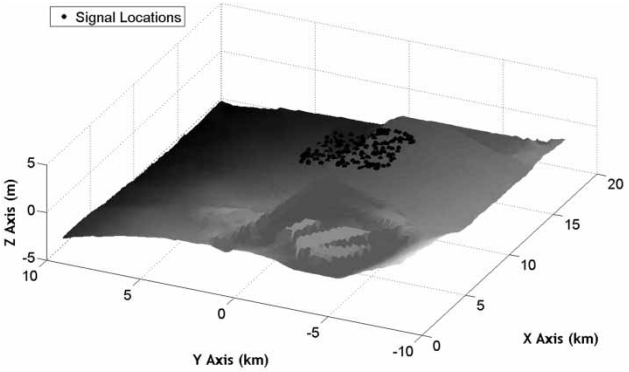

Fig. 2 Location of signal sources – baseline configuration (200 signal sources, $\sigma = 0.0001$, $b = 0.3$ m)

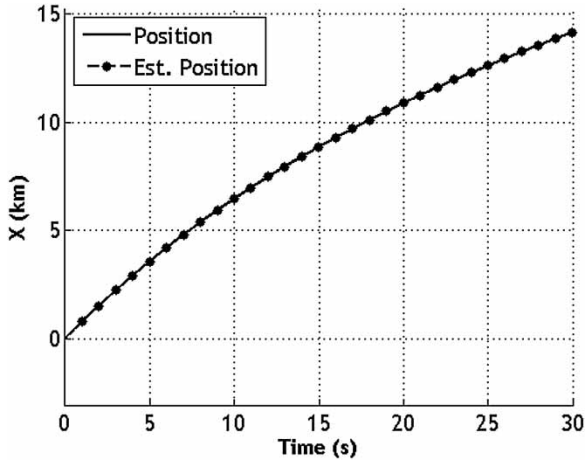

Fig. 3 Range versus time for example trajectory – baseline configuration (200 signal sources, $\sigma = 0.0001$, $b = 0.3$ m)

seen in Table 1. Figures 3 to 5 show the navigation solution for position using the algorithm discussed above. Notice that the estimated position is only plotted every second, but in fact is calculated every 0.01 s. Additionally, if the navigation solution was used as part of a feedback control system, the delay in computing the position and velocity would need to be considered. From these three plots, one can deduce that a relatively accurate navigation solution is generated in this case. Figure 6 provides the 3D trajectory of the projectile along with the location of the 200 ground-based RF signals. To better demonstrate the correlation between distance from signal sources and accuracy, the residual of the position calculations is plotted in Fig. 7, where the residual is the absolute value of the difference between the actual position and estimated position. Note that the X and Y residuals follow a similar trend and decrease as the projectile approaches the target and concentration of signal sources. However, the Z residual tends to deviate from this trend near the target. The divergence in both the altitude and altitude rates is based on the fact that the projectile is directly over the signal sources, which means

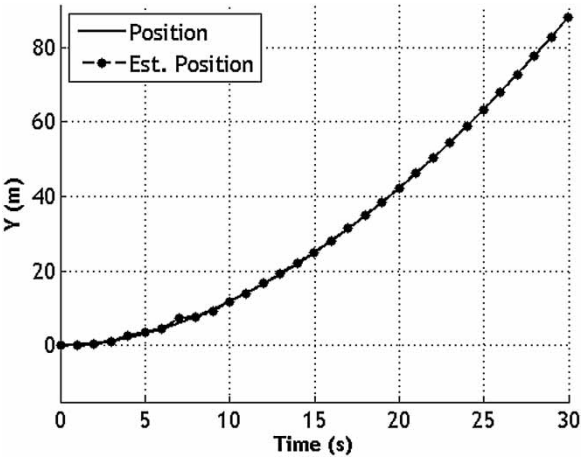

Fig. 4 Cross range versus time for example trajectory – baseline configuration (200 signal sources, $\sigma = 0.0001$, $b = 0.3$ m)

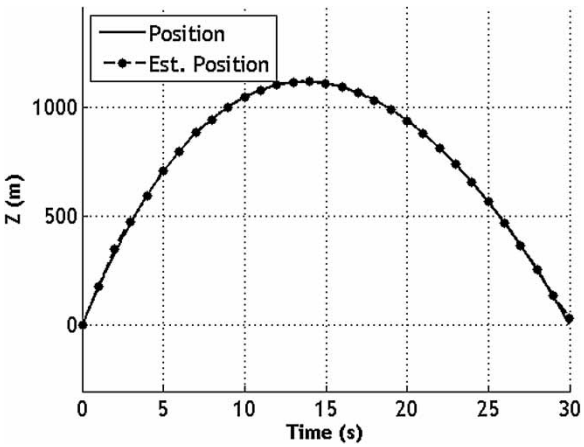

Fig. 5 Altitude versus time for example trajectory – baseline configuration (200 signal sources, $\sigma = 0.0001$, $b = 0.3$ m)

that there is very little deviation in the range information because these signal sources are located on flat land. This phenomenon is further studied in the trade studies section of this article. Figure 8 graphs the velocity residuals throughout the entire trajectory, and as expected, the velocity residuals follow similar trends as the position residuals.

To explore more general characteristics of the navigation solution, Monte Carlo simulations were utilized and examples of Monte Carlo simulation results are documented in Figs 9 to 12. For this simulation, 50 RF ground-based signal sources provided sensor data to the projectile to create a navigation solution. These signal sources are randomly distributed over an 18 km $\times$ 18 km grid. For each signal source, the standard deviation for the noise and bias were $\sigma = 0.0001$ and $b = 0.3$ m, respectively. The standard deviation for signal source X and Y position error is 1.0 m. A sample size of 1000 was used for all Monte Carlo simulation results. Results are reported at various points

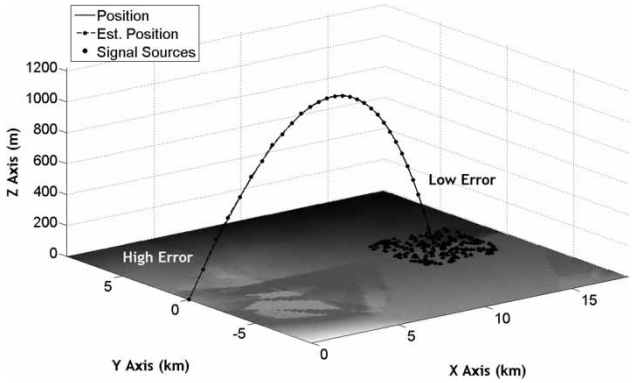

Fig. 6 Example trajectory for baseline configuration (200 signal sources, $\sigma = 0.0001$, $b = 0.3$ m)

along the projectile trajectory from launch (0 per cent) to impact (100 per cent). Figure 9 represents the 3D navigation solution along with the signal source locations. The blocks at 3, 15, and 30 s in Fig. 9 show the location of the projectile along the trajectory at these time instants. Figures 10 to 12 present normalized histograms of the position estimates at 3, 15, and 30 s, along with the actual position and mean of the estimated position. The X and Y position estimates are tightly bounded in all cases. The Z position estimate is also tightly bounded, except for near the target where the estimate deteriorates. The lowest standard deviation of the position estimates is generally when the projectile is above the centre of the signal cluster.

5 PARAMETRIC TRADE STUDIES

In order to probe the performance of this navigation solution method, navigation solution accuracy is studied as a function of different system characteristics including signal source grid size and density, signal source error levels and terrain characteristics. A baseline configuration is considered with 50 signal sources randomly placed over an 18.3 km $\times$ 18.3 km terrain map. The range and range rate error characteristics are $\sigma = 0.0001$ and $b = 0.3$ m. The signal source position error standard deviation is 1 m in both the X and Y directions. Accuracy of the navigation solutions is defined using a 95 per cent confidence sphere (radius that encompasses 95 per cent of all the navigation solutions at that point in the trajectory). The same metric was used to describe the accuracy of the estimated velocity.

Three different terrain environments were considered using actual elevation data. These were used to simulate flat land, mountains, and an urban landscape. Three-dimensional surface plots for these elevation data sets are shown in Figs 13 to 15. The Bonneville Salt Flats in Fig. 13 have a maximum altitude of 3.7 m and minimum altitude of -2.7 m, which provides very little variation in the altitude of the

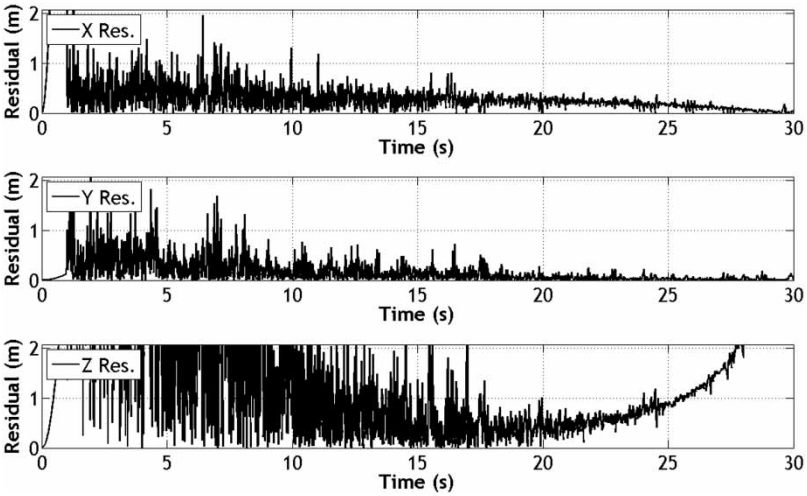

Fig. 7 Position residuals versus time for example trajectory – baseline configuration (200 signal sources, $\sigma = 0.0001$, $b = 0.3$ m)

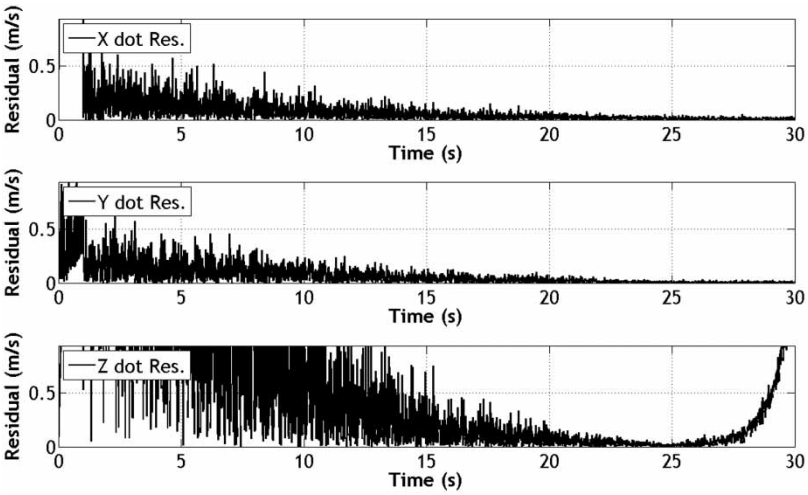

Fig. 8 Velocity residuals versus time for example trajectory – baseline configuration (200 signal sources, $\sigma = 0.0001$, $b = 0.3$ m)

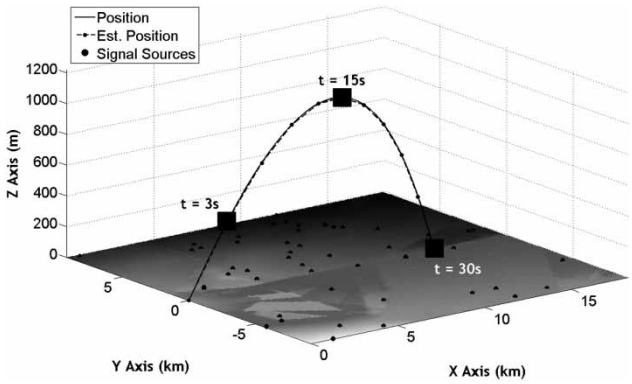

Fig. 9 Three-dimensional trajectory with elevation data and areas of focus: 3, 15, and 30 s

ground-based signals. It is representative of flat land. The opposite is the case for the mountainous terrain of Colorado shown in Fig. 14, which has a maximum altitude of 257.2 m and minimum altitude of −356.4 m. This is representative of mountain terrain. The last landscape depicted in Fig. 15 is the elevation data set for the city of Atlanta, Georgia, which has a maximum altitude of 78 m and a minimum altitude of −38.4 m. It is representative of urban terrain.

The effect of the RF ground-based signal's grid size is explored in Figs 16 and 17. Six different square grid sizes were evaluated, at sizes of 0.3, 1.5, 3.0, 6.1, 9.1, and 12.2 km. Each grid was located at the centre of the trajectory. Figure 16 displays the confidence spheres for estimating the position at 3, 15, and 30 s. As expected, by increasing the grid size, the accuracy of the navigation solution improves with the best performance arising from the mountain landscape. At time equal to 15 s, the projectile is directly over the centre of the grids, which is why little improvement is noticed by increasing grid size. When the projectile is about to impact the ground, there is still an improvement

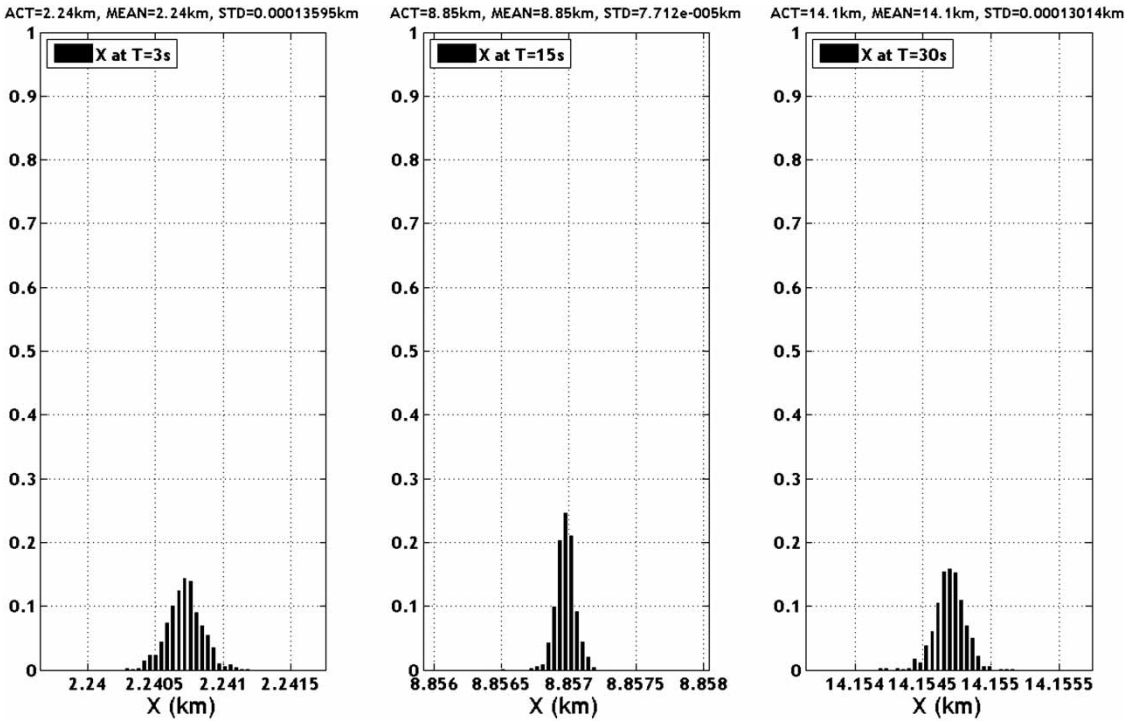

Fig. 10 Histograms of X calculated at $t = 3$, 15, and 30 s – Monte Carlo simulation

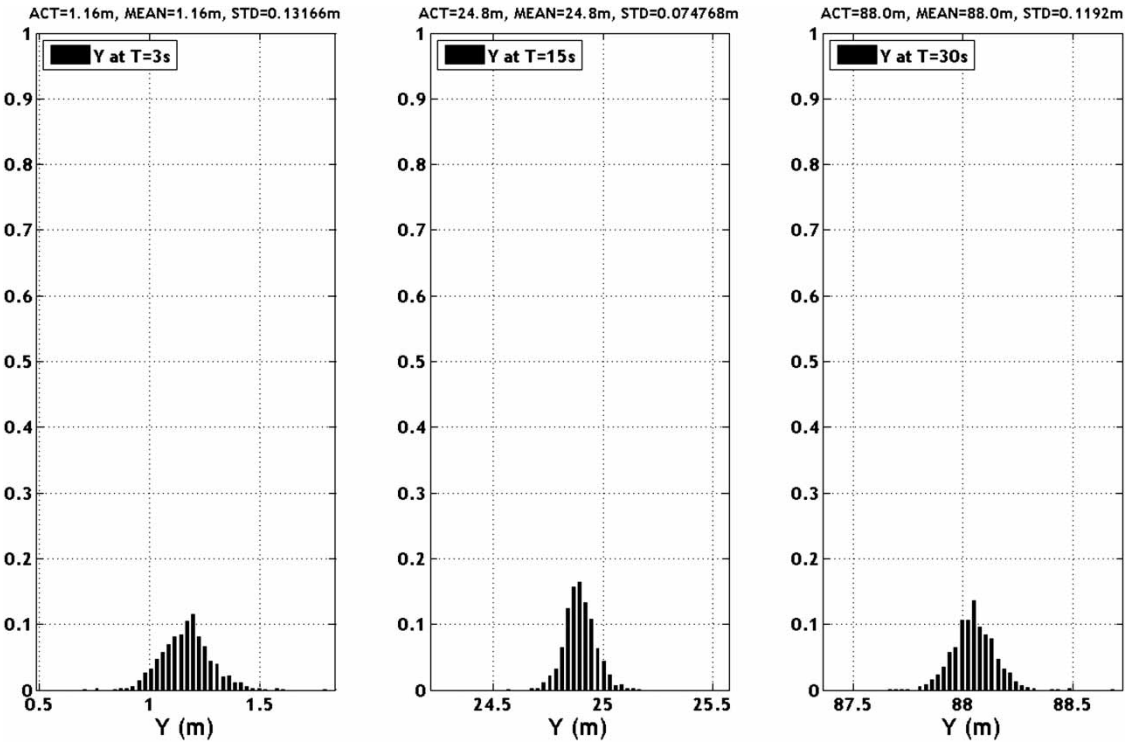

Fig. 11 Histograms of Y calculated at $t = 3$, 15, and 30 s – Monte Carlo simulation

for the mountain and urban landscapes, but not for the flat ground. This phenomenon is attributed to the fact that there is little variation in the altitude of the signal sources. Identical trends are seen in Fig. 17 for estimating velocities, with largest confidence spheres occurring near the target.

In order to study the density of ground-based SOOP, a trade study was performed varying the number of signals available. The numbers of signals considered were 25, 50, 100, 150, 200, 300, 400, and 500. Figure 18 displays the confidence spheres for estimated position, and interestingly at $t = 3$ s the

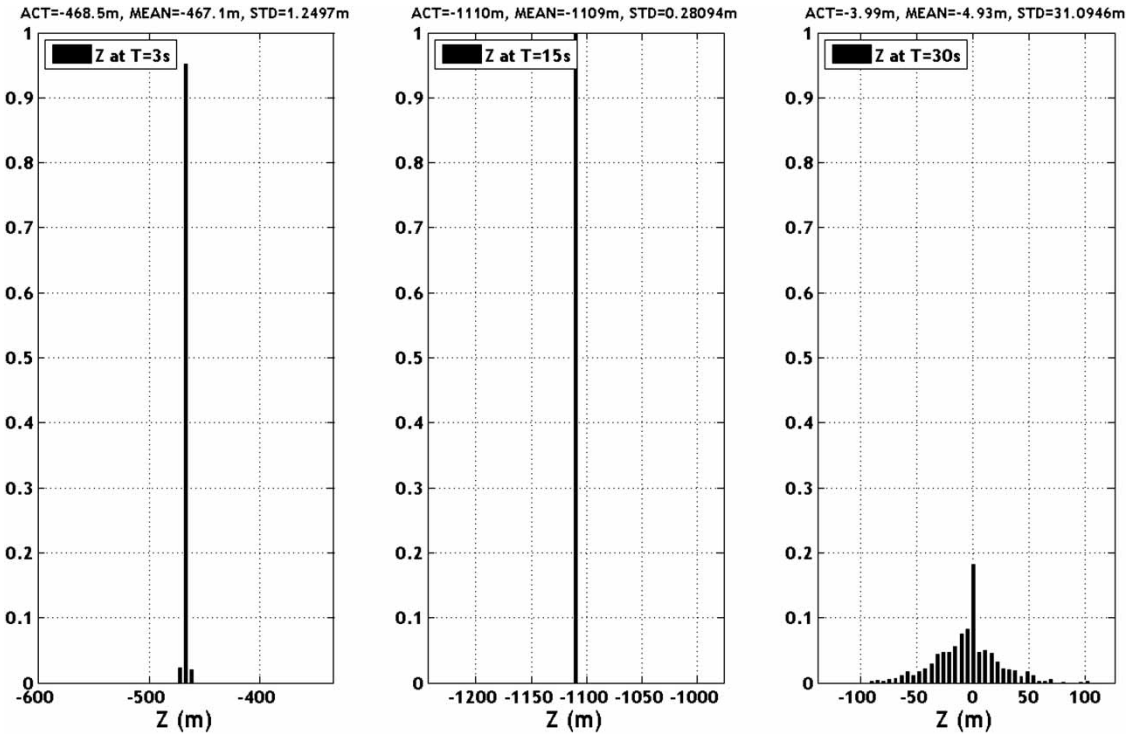

Fig. 12 Histograms of Z calculated at $t = 3$, 15, and 30 s – Monte Carlo simulation

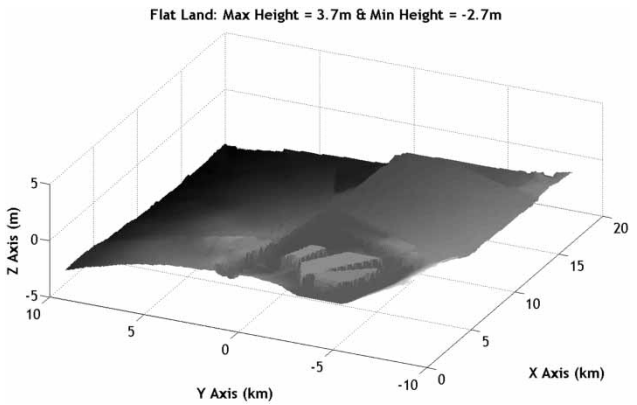

Fig. 13 NED data set for Bonneville Salt Flats in Utah (flat landscape)

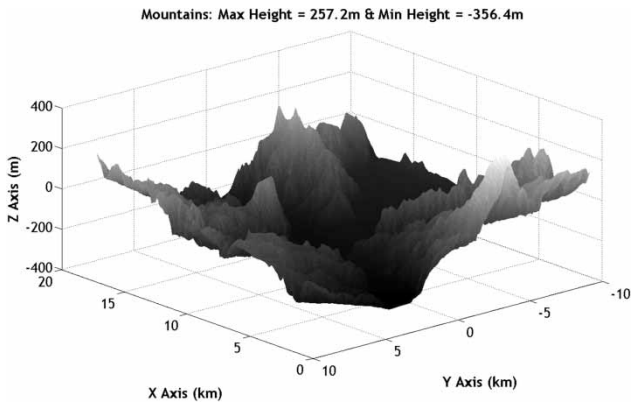

Fig. 14 NED data set for Colorado mountains (mountain landscape)

accuracy is directly correlated to the number of SOOP available, but only to a certain level. Beyond 200 signal sources, accuracy asymptotically approaches a limit. This same trend can be seen at $t = 15$ s, but on a smaller scale. However, accuracy near the target is degraded by the loss of line of sight, reduced visibility, and decreased signal sources. Similar trends can be seen in Fig. 19, which plots the velocity confidence spheres as a function of the number of initial signal sources.

Ground location of the signals relative to the trajectory plays an important role in accuracy, which is why a parametric trade study evaluated the effect of the signal sources' location on accuracy of the navigation solution. Four main signal locations were selected

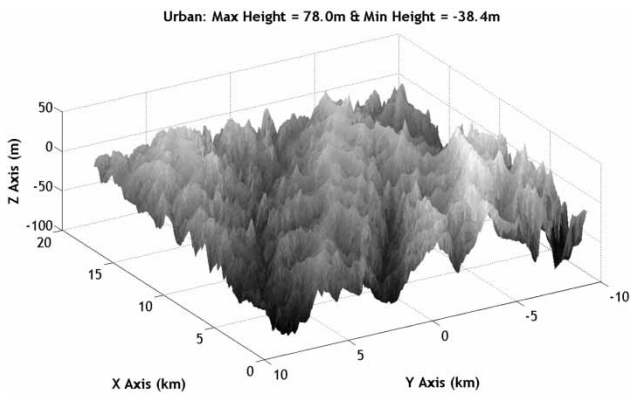

Fig. 15 NED data set for Atlanta, Georgia (urban landscape)

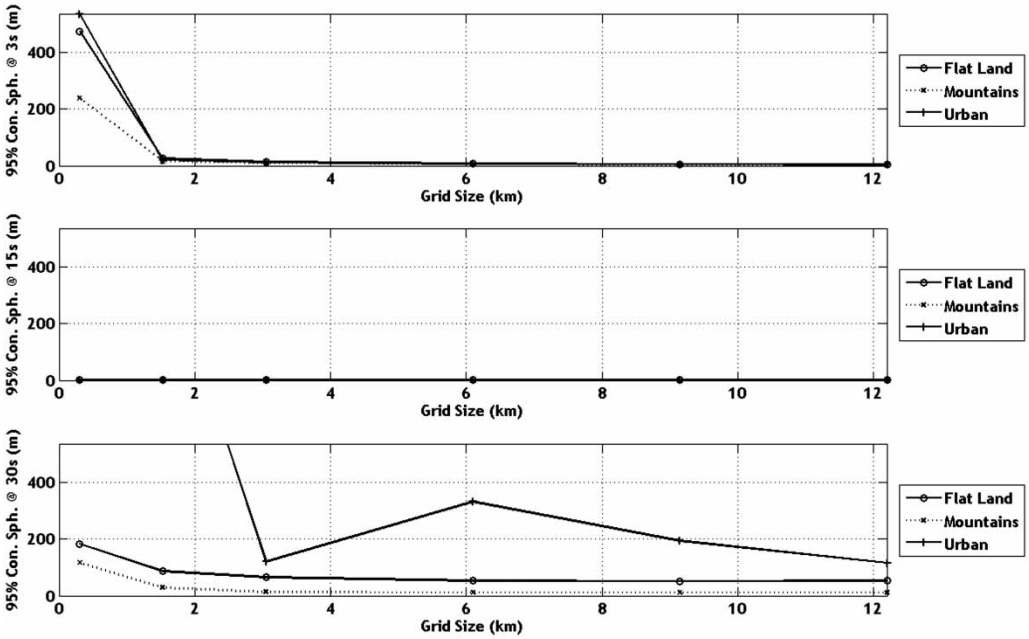

Fig. 16 Ninety-five per cent confidence position spheres versus grid size for 3, 15, and 30 s

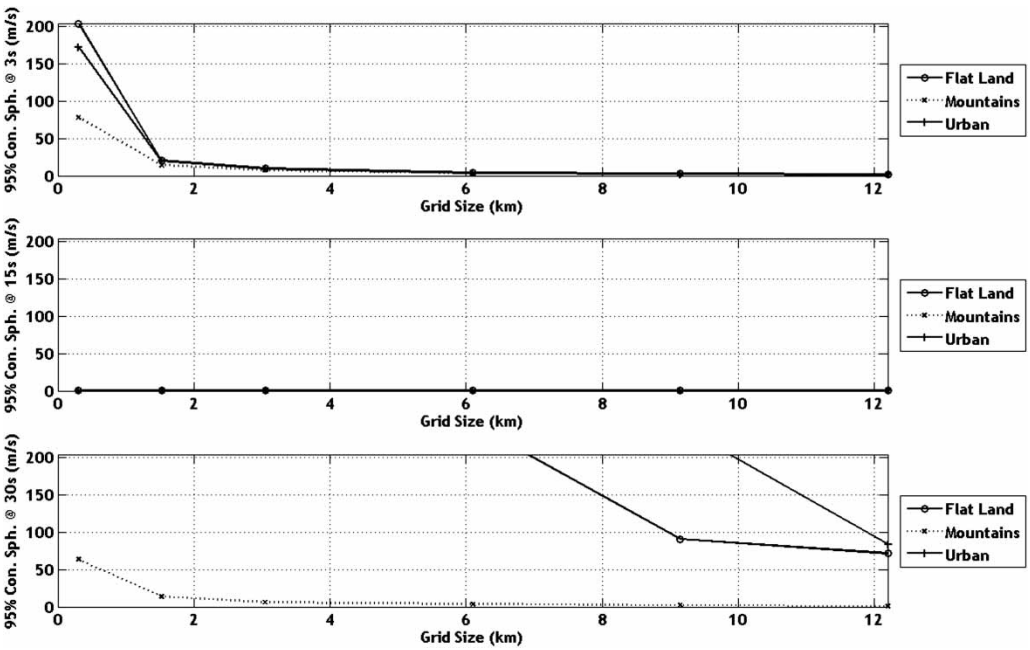

Fig. 17 Ninety-five per cent confidence velocity spheres versus grid size for 3, 15, and 30 s

for this parametric trade study and these were located near the muzzle, directly east of the middle of the trajectory, directly west of the middle of the trajectory, and centred at the impact point. A grid size of 6.1 km $\times$ 6.1 km grid was assumed. The results for this trade study are given in Table 2. At $t = 3$ s, the grids located near the gun provide the best navigation solution being that these signals are closer to the projectile at this instant in time. When the projectile is 15 s into flight, all four locations performed relatively the same, which is attributed to the fact that all the SOOP have a direct line of sight and the projectile is relatively the same distance from each signal source grid. Similar to the case when $t = 3$ s, the navigation solution at 30 s is best determined by the grid located near the impact point. Based on this trade study, it is apparent that the navigation solution is best calculated when the projectile is directly over the centre of the signal source grid.

A major factor driving the accuracy of navigation solution is the error level value σ, which varies depending on which type signal source is implemented.

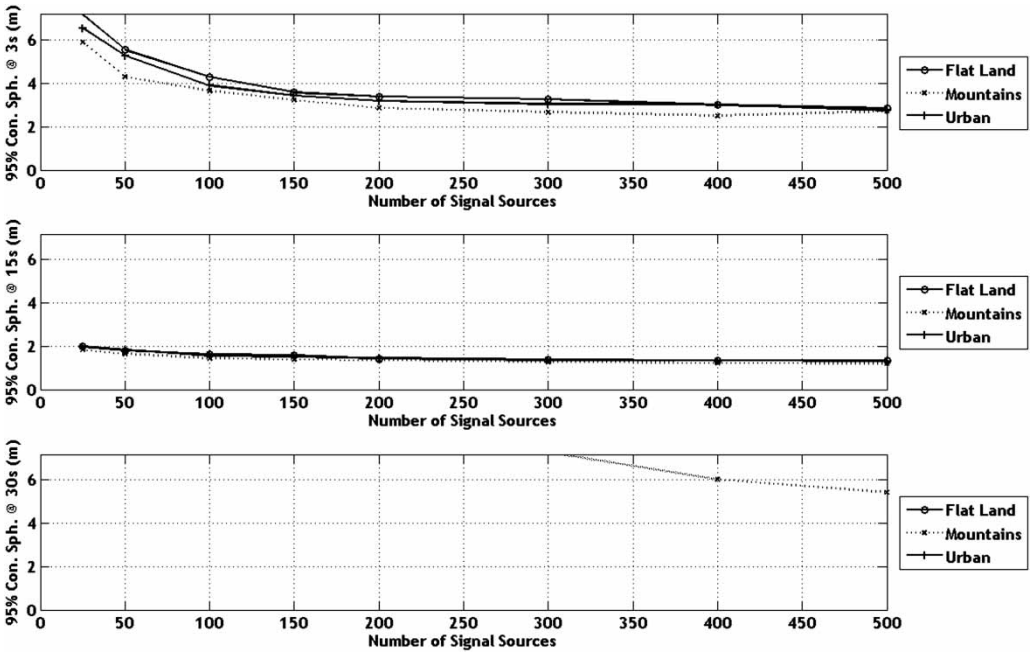

Fig. 18 Ninety-five per cent confidence position spheres versus number of signal sources for 3, 15, and 30 s

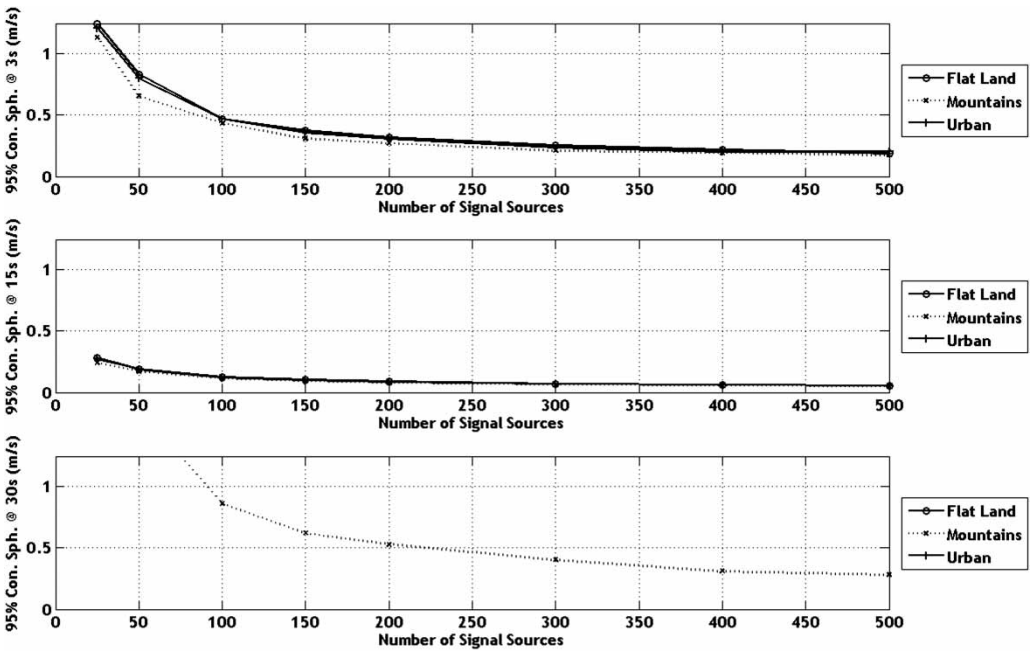

Fig. 19 Ninety-five per cent confidence velocity spheres versus number of signal sources for 3, 15, and 30 s

Experimental values for this error source and the corresponding type of signal are given in Table 1. Using this table as a guide, the effect of error level on accuracy was varied for values of 0.0001, 0.0005, 0.001, 0.005, and 0.01, while holding all other characteristics at nominal levels specified above. It is expected that as error levels increase, accuracy decreases. At $t = 3$ s and $t = 15$ s, there tends to be a linear relationship between error levels and confidence spheres, which can be seen in Fig. 20. However, near the impact point, the position confidence spheres are corrupted due to the loss of signals and or minimized altitude variation. Figure 21 also demonstrates this property with relation to velocity estimations.

An obvious error source is inaccurate knowledge of the location of the signal source. In order to understand how this error source affects estimation accuracy, signal source X and Y positions were randomly

Table 2 Ninety-five per cent confidence spheres versus location of signal sources for 3, 15, and 30 s

		Flat				Mountains				Urban			
	Time (s)	South	East	West	North	South	East	West	North	South	East	West	North
Position (m)	3	1.0	18.1	18.7	54.4	0.8	17.0	10.4	27.6	0.9	15.4	15.1	49.9
	15	2.2	2.5	2.4	2.8	1.7	2.2	1.9	2.4	2.2	2.3	2.3	2.5
	30	36.4	13.6	12.5	1.2	16.7	7.87	7.06	0.8	30.3	12.2	11.0	1.1
Velocity (m/s)	3	0.2	6.9	6.8	19.4	0.2	7.1	4.0	10.9	0.3	6.7	5.8	18.6
	15	0.9	0.4	0.4	1.2	0.8	0.3	0.3	1.0	0.9	0.4	0.3	1.1
	30	6.9	1.8	1.6	0.1	3.1	1.1	0.9	0.1	6.2	1.6	1.5	0.1

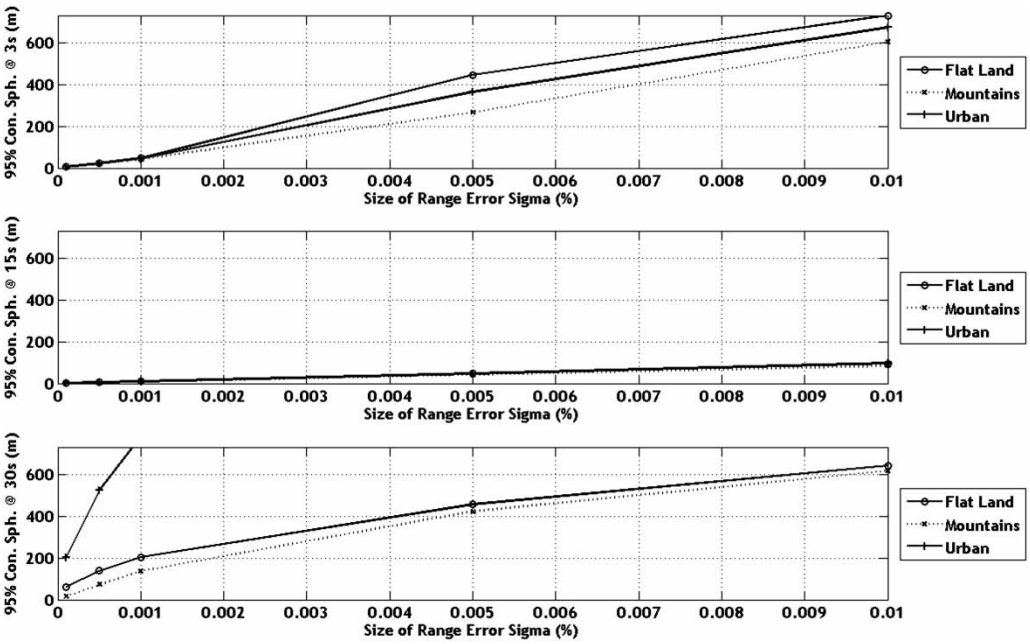

Fig. 20 Ninety-five per cent confidence position spheres versus size of error level for 3, 15, and 30 s

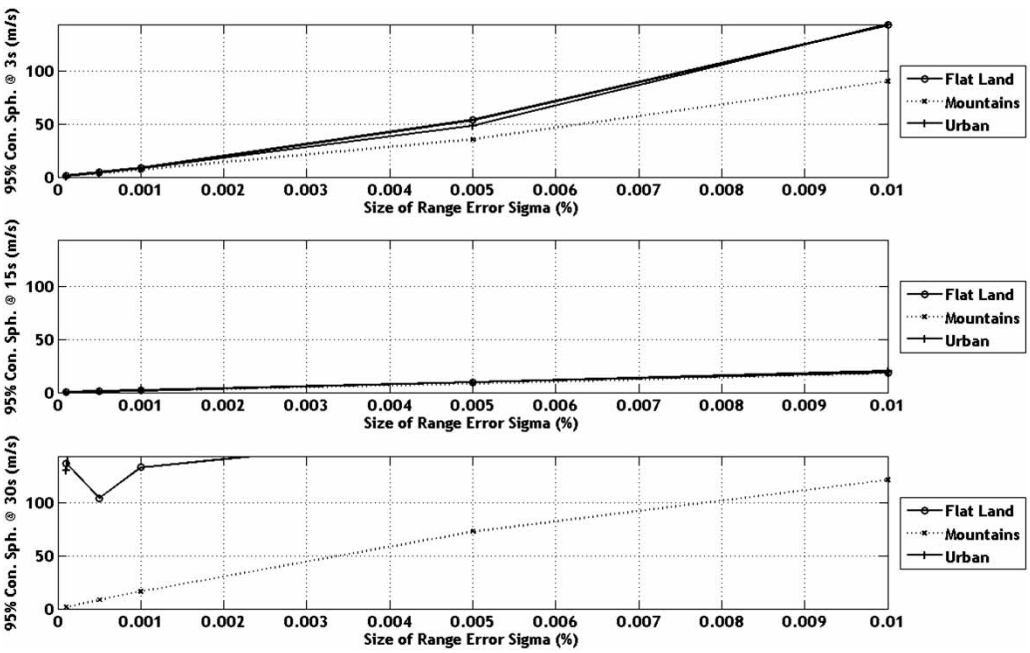

Fig. 21 Ninety-five per cent confidence velocity spheres versus size of error level for 3, 15, and 30 s

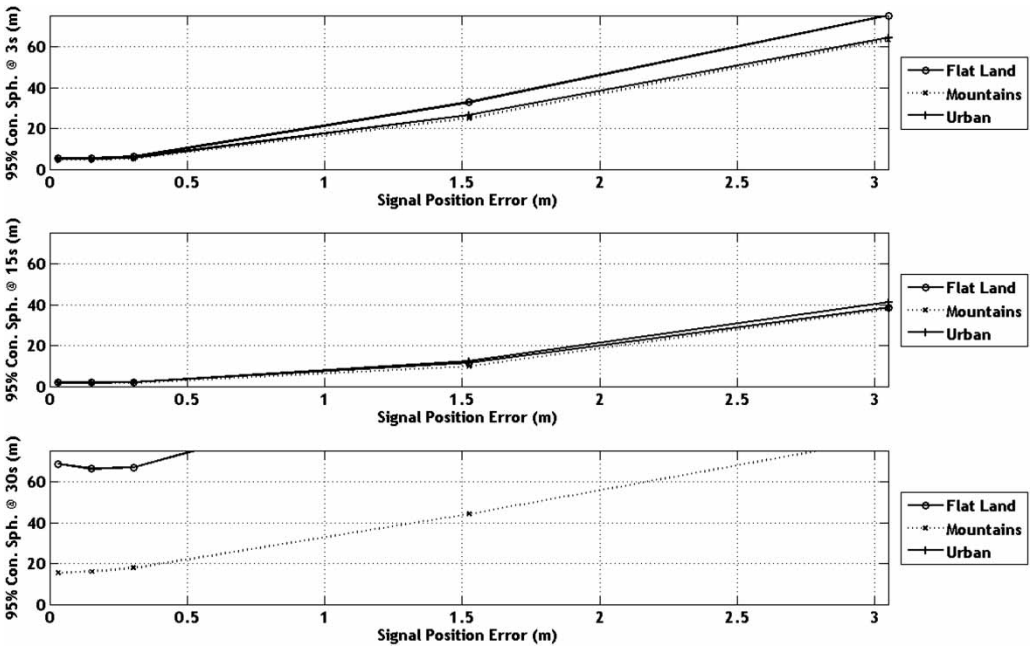

Fig. 22 Ninety-five per cent confidence position spheres versus error in signal source position for 3, 15, and 30 s

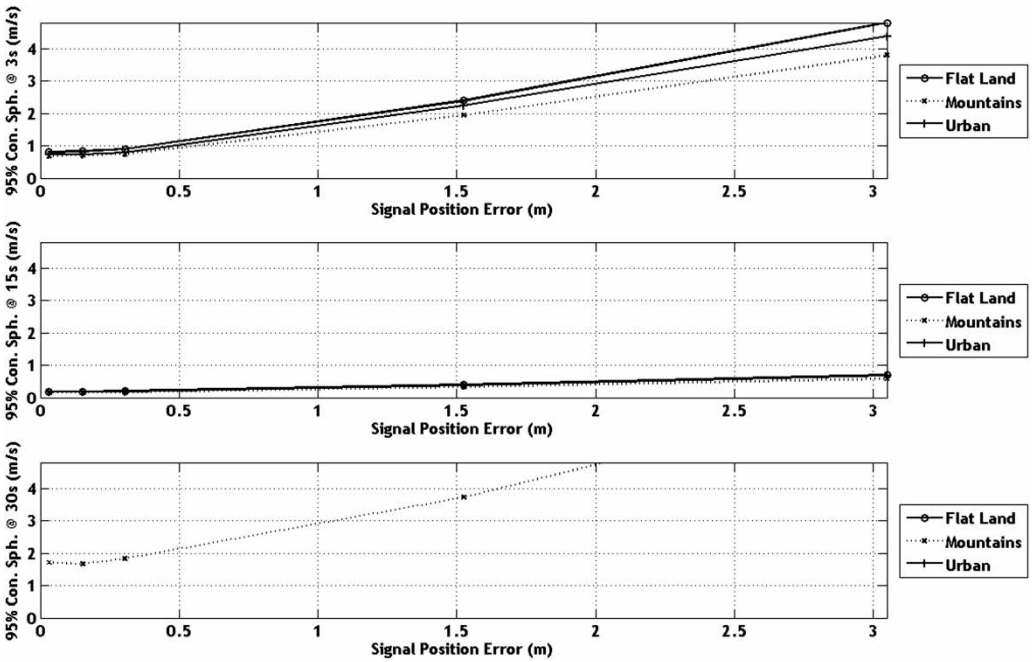

Fig. 23 Ninety-five per cent confidence velocity spheres vs. error in signal source position for 3, 15, and 30 s

perturbed from their actual location by a standard deviation of 0.03, 0.15, 0.3, 1.5, and 3 m. Similar to the previous parametric trade study on error levels, there tends to be an overall upward trend correlating to increasing estimation errors due to increasing signal source position errors, which is displayed in Fig. 22. The same is true for velocity estimations in Fig. 23.

Based on the parametric trade studies documented in this section and previously reported work, a set of mission profiles were selected to demonstrate a best, medium, and worst case scenario. Each scenario was performed on all three elevation data sets, and the signal sources were centred at the target in a 4.6 km^2. The values selected for the best case were 200 signal sources with error levels $\sigma = 0.0001$ and $b = 0.3$ m, and signal source misposition of 0.3 m. For the medium scenario, 100 signal sources were used with error levels of $\sigma = 0.001$ and $b = 1.5$ m, and signal

Table 3 Ninety-five per cent confidence spheres versus scenarios for 3, 15, and 30 s

		Flat			Mountains			Urban		
	Time (s)	Best	Medium	Worst	Best	Medium	Worst	Best	Medium	Worst
Position (m)	3	12.3	207.9	1470	9.9	103.7	1271	11.9	227.7	1413
	15	3.0	20.1	579.9	2.7	16.3	323.5	3.1	17.9	564.1
	30	1.7	6.5	35.5	1.4	4.8	25.6	1.7	6.3	32.3
Velocity (m/s)	3	3.5	56.6	5170	2.8	40.6	1334	3.6	56.3	4144
	15	0.5	7.3	193.3	0.5	6.4	148.4	0.5	6.8	181.9
	30	0.1	1.0	18.7	0.1	0.7	13.5	0.1	0.9	308.3

source misposition of 1.5 m. The worst case consisted of only 25 signal sources with $\sigma = 0.01$ and $b = 3$ m error levels, and a signal source misposition of 3 m. The results for $t = 3$, 15, and 30 s are shown in Table 3. As expected, the best case scenario significantly outperformed the two additional scenarios. With respect to elevation data sets, the mountainous landscape outperformed the remaining landscapes, mainly due to the fact that it allowed the altitude of signal sources to vary the most. Taking the best case scenario metrics into consideration, the best case scenario is capable of producing results similar to GPS-driven navigation solutions [**26**, **27**].

6 CONCLUSION

A general method was created to evaluate the ability of ground-based range and range rate information to be used by a projectile to construct a navigation solution. Systematic studies were performed to better understand the merits and demerits of this type of system to create a useful navigation solution. Based on these studies, highly accurate navigation solutions stem from relatively large variations in altitude among the signal sources, typically on the order of tens of metres. Also, this variation should also be applied to X and Y positioning of signal sources, but with a concentration around which the navigation solution needs to be the most accurate, which is typically near the target for smart projectiles. The number of RF ground-based signal sources plays an important role in accuracy; however, there is certainly a point of diminishing return. A cluster of properly placed, currently available, ground-based RF signals are able to produce navigation solutions equal in accuracy to GPS and can be used as a practical navigation solution when GPS is not available.

REFERENCES

1 **Parsch, A.** Texas instruments paveway I & Pave storm. Directory of U.S. Military Rockets and Missiles, 2006 (Texas Instruments, Munich, Germany).

2 **Parsch, A.** Boeing (McDonnell Douglas) JDAM. Directory of U.S. Military Rockets and Missiles, 2006 (Texas Instruments, Munich, Germany).

3 **Abbott, A.** Antijamming and GPS for critical military applications. Crosslink, Aerospace Corporation, Summer 2002.

4 Defense Update. GPS Anti-Jam Receiver (AGR). Defense Update, 26 January 2005.

5 **Williams, P., Basker, S.,** and **Ward, N.** ENavigation and the case for eLORAN. *J. Navig.*, 2008, **61**, 473–484.

6 **Savarese, C., Rabaey, J.,** and **Beutel, J.** Locationing in distributed *ad-hoc* wireless sensor networks. In Proceedings of the 2001 IEEE International Conference on *Acoustics, speech, and signal processing*, Salt Lake City, Utah, 2001, vol. 4, pp. 2037–2040.

7 **Yang, P., Wu, W., Moniri, M.,** and **Chibelushi, C. C.** SLAM algorithm for 2D object trajectory tracking based on RFID passive tags. In Proceedings of the IEEE International Conference on *RFID*, Las Vegas, Nevada, 2008, pp. 165–172.

8 **Bekkali, A., Sanson, H.,** and **Matsumoto, M.** RFID indoor positioning based on probabilistic RFID map and Kalman filtering. In Proceedings of the Third IEEE International Conference on *Wireless and mobile computing, networking and communications*, White Plains, New York, 2007, pp. 21–21.

9 **McEllroy, J.** *Navigation using signals of opportunity in the AM transmission band*. Thesis, Air Force Institute of Technology, 2006.

10 **Crosby, J. G.** *Fusion of inertial sensors and orthogonal frequency division multiplexed (OFDM) signals of opportunity for unassisted navigation*. Thesis, Air Force Institute of Technology, 2009.

11 **Martin, R. K., Velotta, J. S.,** and **Raquet, J. F.** Bandwidth efficient cooperative TDOA computation. *IEEE Trans. Signal Process.*, 2009, **57**(6), 2311–322.

12 Enhanced Loran (eLoran). *Issue brief*, 0.1th edition, 2007 (International Loran Association, Santa Barbara, California).

13 The Case for eLORAN. Technical report, General Lighthouse Authorities of the United Kingdom and Ireland, 2006.

14 **Offermans, G., Helwig, A., Williams, P.,** and **Pelgrum, W.** Differential eLoran trials in Harwich harbour. In Proceedings of the 35th ILA Convention, Groton, 23 October 2006, Lecture.

15 **Lymberopoulos, D., Lindsey, Q.,** and **Savvides, A.** An empirical characterization of radio signal strength variability in 3-D IEEE 802.15.4 networks using monopole antennas. Technical report, Yale University, 2006.

16 Ash, J. N. and **Potter, L. C.** Sensor network localization via received signal strength measurements with directional antennas. Technical report, Ohio State University, 2004.

17 Fisher, K. *The navigation potential of signals of opportunity-based time difference of arrival measurements*. Thesis, Air Force Institute of Technology, 2005.

18 McEllroy, J., Raquet, J. F., and **Temple, M. A.** Opportunistic navigation. *GPS World*, 1 July 2007.

19 Misra, P. and **Enge, P.** *Global positioning system: signals, measurements, and performance*, 2006 (Ganga-Jamuna, Lincoln, Massachusetts).

20 Hall, T. *Radiolocation using AM broadcast signals*. Thesis, Massachusetts Institute of Technology, 2002.

21 Griva, I., Nash, S., and **Sofer, A.** *Linear and nonlinear optimization*, 2009 (Society for Industrial and Applied Mathematics, Philadelphia).

22 Gill, P. E., Murray, W., and **Wright, M. H.** *Practical optimization*, 1981 (Academic, London).

23 Brian, M. and **Harris, T.** How GPS receivers work. *HowStuffWorks*, Web, available from http://electronics.howstuffworks.com/gadgets/travel/gps2.htm.

24 Kaminsky, A. *Trilateration*, 2007 (Rochester Institute of Technology, Rochester, New York).

25 Gast, R., Morris, S., and **Costello, M.** Simulation of shot impacts for the M1A1 tank gun. *J. Guid. Control Dyn.*, 2000, **23**(1), 53–59.

26 Xu, G. *GPS: theory, algorithms, and applications*, 2007 (Springer, Berlin).

27 El-Rabbany, A. *Introduction to GPS the global positioning system*, 2nd edition, 2006 (Artech House, Norwood, Massachusetts).

APPENDIX

Notation

b_i	Gaussian bias term
$\boldsymbol{E}_k$	error vector
$\bar{\boldsymbol{I}}_{\mathrm{I}}, \bar{\boldsymbol{J}}_{\mathrm{I}}, \bar{\boldsymbol{K}}_{\mathrm{I}}$	inertial reference frame unit vectors
J_k	Jacobian of the kth iteration
$\boldsymbol{P}_k$	vector of the kth unknown parameters
$\bar{\boldsymbol{r}}_{o\rightarrow p}$	distance vector from origin of the inertial reference frame to the mass centre of the projectile
$\bar{\boldsymbol{r}}_{o\rightarrow s_i}$	distance vector from origin of the inertial reference frame to the ith signal source
R_i	range from the ith signal source to the projectile
$\tilde{R}_i$	pseudorange from the ith signal source to the projectile
$\dot{R}_i$	range rate from the ith signal source to the projectile
$\dot{\tilde{R}}_i$	pseudorange rate from the ith signal source to the projectile
$\bar{\boldsymbol{v}}_{\mathrm{P/I}}$	translational velocity of the mass centre of projectile in the inertial reference frame
$\bar{\boldsymbol{v}}_{S_i/\mathrm{I}}$	translational velocity of the ith signal source in the inertial reference frame
w_i	Gaussian random number
x, y, z	position vector components of the composite body centre of mass expressed in the inertial reference frame
$x_{s_i}, y_{s_i}, z_{s_i}$	position vector components of the ith signal source expressed in the inertial reference frame
$\dot{x}, \dot{y}, \dot{z}$	velocity vector components of the composite body centre of mass expressed in the inertial reference frame
$\dot{x}_{s_i}, \dot{y}_{s_i}, \dot{z}_{s_i}$	velocity vector components of the ith signal source expressed in the inertial reference frame
α_k	line search parameter
σ_i	standard deviation of noise